

Design and Radiation Assessment of Optoelectronic Transceiver Circuits for ITER

P. Leroux^a, W. De Cock^b, M. Van Uffelen^b, M. Steyaert^c

^aKatholieke Hogeschool Kempen, ICT-RELIC, Kleinhoefstraat 4, B-2440 Geel, Belgium.

^bSCK-CEN, the Belgian Nuclear Research Centre, Boeretang 200, B-2400 Mol, Belgium.

^cKatholieke Universiteit Leuven, ESAT-MICAS, Kasteelpark Arenberg 10, B-3001 Heverlee, Belgium.

Abstract

The presented work describes the design and characterization results of different electronic building blocks for a MGy gamma radiation tolerant optoelectronic transceiver aiming at ITER applications. The circuits are implemented using the 70GHz f_T SiGe HBT in a 0.35 μ m BiCMOS technology. A VCSEL driver circuit has been designed and measured up to a TID of 1.6 MGy and up to a bit rate of 622Mbps. No significant degradation is seen in the eye opening of the output signal. On the receiver side, both a 1GHz, 3k Ω transimpedance and a 5GHz Cherry-Hooper amplifier with over 20dB voltage gain have been designed.

I. INTRODUCTION

One of the most challenging environments with respect to ionizing radiation current electronic designers are facing is ITER (International Thermonuclear Experimental Reactor). In this nuclear fusion reactor, the requirements of integrated electronic circuits with respect to radiation tolerance are very severe. One of the applications in ITER where the radiation conditions are extreme is the maintenance of the diverter. This periodic task will need to be performed by remotely operated robots and its functionality could be improved by adopting a significant amount of on-board electronics. Several systems and circuits will need to remain operational even after exposure to a TID (Total Ionizing Dose) in the order of MGy. The anticipated gamma radiation levels are similar to those expected in the S-LHC. The design of these circuits is clearly very challenging. This paper will focus on the potential use of a bidirectional fiber optic communication link between the robotics operated inside the reactor vessel and the control room. More specifically we will present and discuss our recent results on the design and assessment of the radiation hard optical transceiver electronics. All circuits are designed in a 0.35 μ m BiCMOS technology.

Fig. 1 shows the schematic of a typical fibre optic link including the analogue front-end circuitry for both the transmitter and the receiver side. In previous work we designed and assessed a discrete driver for a VCSEL [6] on the transmitter side of the link. Even though this driver was sufficiently tolerant to radiation, it featured several shortcomings owing to its discrete nature: the inherent frequency performance is limited due to large circuit board parasitics, the complete circuit is rather area consuming which may complicate the mounting of the transmitter and the poor matching performance between the devices in circuit blocks

like a differential pair and a current mirror limits the predictability and hence, the reliability of the driver.

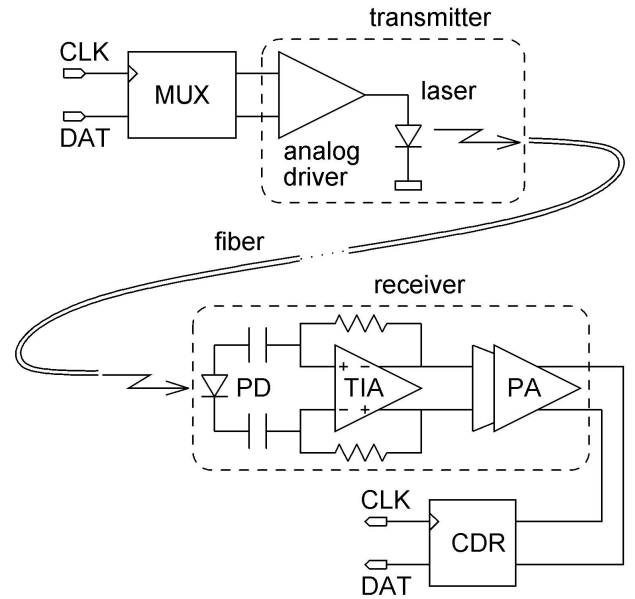


Fig. 1: Fibre optic communication link showing the implemented transmitter and receiver circuits.

The following transmitter section describes the design, simulation and measurement of a new and integrated VCSEL driver in a 0.35 μ m SiGe BiCMOS technology which no longer suffers previous shortcomings. The driver will operate at a power supply of 3.3 V and is intended to be used in combination with a 1550 nm VCSEL. The design is based on SPICE simulations using the model provided by the manufacturer but modified to include the dose dependent effects of gamma irradiation on the devices' DC parameters. In the case of the driver, where only HBT's are used, the model describes the influence of radiation on the base current of the SiGe HBT. Details on the model adaptations for this device are available in [12]. The model itself is based on a similar approach for a discrete SiGe HBT presented in [5].

On the receiver side several electronic building blocks have been designed in the same 0.35 μ m BiCMOS technology. The TIA (TransImpedance Amplifier) is the first block after the photodiode and converts the diode current into a voltage, sufficiently high above the noise floor of the subsequent PA (PostAmplifier). The TIA features a transimpedance gain of 3k Ω for a 1GHz bandwidth. The equivalent input noise current given by the integrated output noise voltage divided by the transimpedance gain is 0.6 μ A. The circuit was

designed taking transistor radiation effects into account. We included the previously measured degradation in the simulation via a DC SPICE model extension of the bipolar transistors. For the PA a sequence of differential bipolar Cherry-Hooper amplifiers was designed with a simulated bandwidth of 5GHz and a gain of 20dB per stage. These receiver circuits are currently being processed.

II. OPTICAL TRANSMITTER

For the transmitter side a driver was implemented for a long wavelength (1550 nm) VCSEL (Vertical Cavity Surface Emitting Laser). The schematic of the integrated VCSEL driver circuit is shown in Fig. 2 and is based on the discrete driver presented in [6]. The current through the VCSEL is composed of a constant DC current, to which we add a pulsed modulation current provided by the driver. A dummy resistor is placed symmetrically with respect to the VCSEL which improves the AC balance of the circuit since Q_{1a} and Q_{1b} now drive a similar load. Transistor Q_2 acts as a current source which is biased by Q_3 in diode configuration, hence creating a current mirror. R_{C3} is an external potentiometer which allows to set the modulation current to the required level. This was done only once and no adjustment during irradiation is required. The supply is set at 3.3 V.

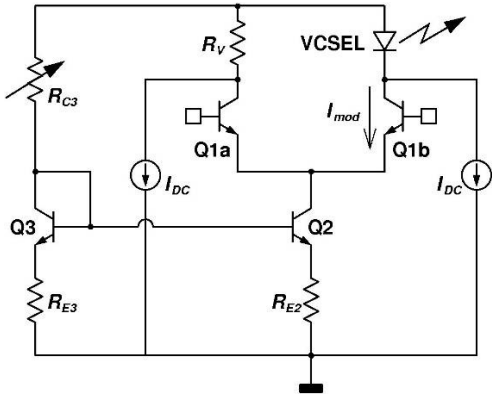


Fig. 2: Schematic of the integrated SiGe VCSEL driver.

The circuit was monitored before, during and after several Co^{60} gamma irradiation experiments up to a TID of 1.6 MGy. Fig. 3 shows the relative increase of the modulation current as a function of the accumulated dose. The modulation current displays a limited variation in the order of 0.1 % up to a dose of 600 kGy. The initial decrease is attributed to an increase in base current for the different transistors as evidenced by separate measurements on identical stand-alone transistors. For Q_3 and Q_2 the additional base current reduces the collector current for both transistors and hence decreases the modulation current through the driver.

The output current through the VCSEL is not only degraded by changes in the base current of Q_2 and Q_3 . A fraction of the current is also lost in the base of Q_{1b} . The initial decrease in modulation current is followed by an increase which is caused by the observed in-situ recovery of the devices during irradiation [12].

The design of the driver could principally be improved to render an even more stable output current, even during

irradiation. The influence of the base current of Q_2 and Q_3 on the output current can be reduced by using an extra emitter follower Q_4 in the current mirror to deliver the base current of both Q_2 and Q_3 . This solution is depicted in Fig. 4. The influence of the base current changes of Q_{1a} and Q_{1b} could be counteracted by using a Darlington pair to substitute both transistors. The obvious downside of this solution is the effective doubling of the input transistors base-emitter voltage.

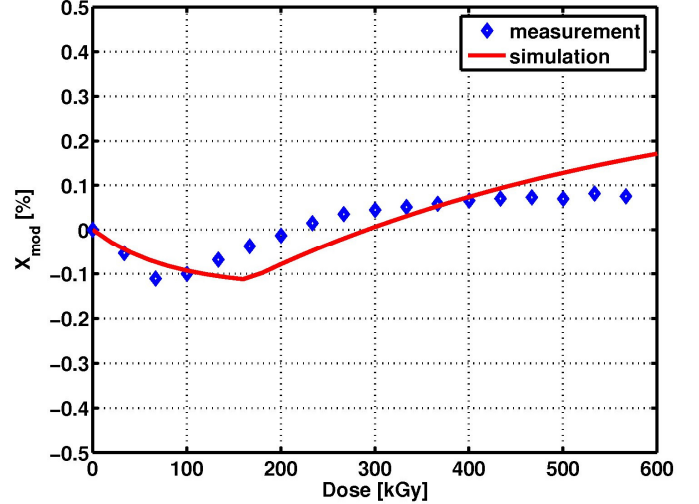


Fig. 3: Modulation current through the VCSEL, measured as a function of the accumulated dose.

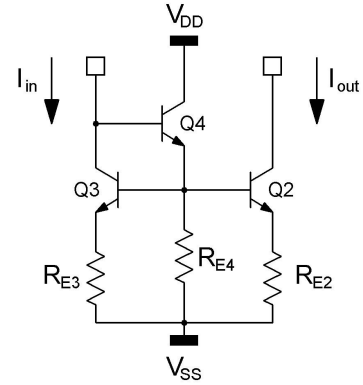


Fig. 4: Improved current mirror topology with reduced current degradation under radiation.

The measurement data have been confirmed with SPICE simulations based on the model described in [12]. The same initial decrease and subsequent increase in modulation current is observed. Note that the minimum in the modulation current, occurring at a dose of 80 kGy does not correspond to the maximum in base current, just before the onset of recovery. This difference may be attributed to a difference in measurement conditions. For the separate devices the pins were grounded between two consecutive measurements during irradiation. This was not possible for the driver where the connections to the different contact switches are much more complex. Also the driver continuously draws a current of a few mA when it is being measured where the devices were measured for a large current range which makes the

average current lower.

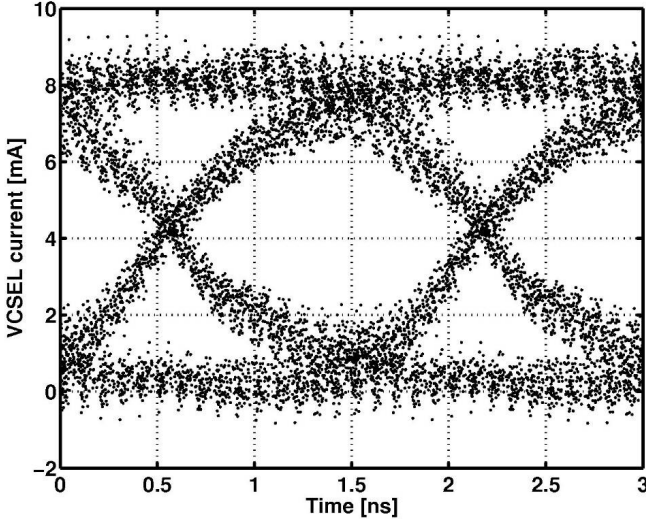


Fig. 5: Eye diagram of modulation current through the VCSEL after a dose of 1.6 MGy at 622 Mbps.

A second irradiation experiment has been performed to verify the operation of the driver up to a TID of 1.6 MGy and up to a bitrate of 622 Mbps. The resulting eye diagram is shown in Fig. 5. A photograph of the integrated driver, within a ceramic DIL40 package is depicted in Fig. 6.

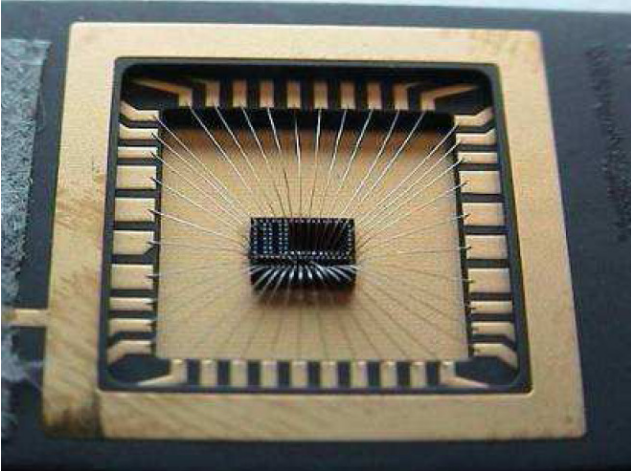


Fig. 6: Photograph of an integrated SiGe VCSEL driver.

III. OPTICAL RECEIVER

Two crucial building blocks in the design of the receiver (Fig. 1) will be discussed: a differential bipolar transimpedance amplifier and a differential bipolar Cherry-Hooper amplifier which is used to construct the postamplifier.

Fig. 7 shows a simplified schematic of the transimpedance amplifier. It consists of a common-base input stage, formed by Q_1 which decouples the input capacitance (including the diode capacitance and parasitic capacitance related to the connections to the IC) from the transimpedance feedback loop. This stage presents a current gain of almost 1. The second stage consists of a common-emitter stage formed by Q_2 with shunt-shunt feedback resistor R_f . The transimpedance gain of the circuit can be approximated by $2R_f$. The bandwidth of the circuit is determined by the base node of Q_2 . On this node, the resistance needs to be sufficiently high to

keep the GBW (gain bandwidth) of the loop sufficiently below the output pole of the open loop system in order to guarantee the system stability:

$$BW = \frac{1 + g_{m2}R_2}{2\pi C_{b2}(R_f \parallel R_1)}. \quad (1)$$

Notice that both for achieving high gain and good stability the value of R_f will be chosen sufficiently high. The low frequency noise contributions referred to the input of the circuit are given by

$$\overline{i_{n,in}^2} = 2kT\Delta f \left(\frac{1}{R_c} + \frac{1}{R_1} + \frac{r_{b1}}{R_c^2} + \frac{1}{R_f} \right), \quad (2)$$

where r_{b1} is the parasitic base resistance of Q_1 . This expression shows the main drawback of adding a common base input stage as it reduces the noise performance by the first three terms in equation (2). Even though R_f can be chosen larger the overall noise performance will still be degraded.

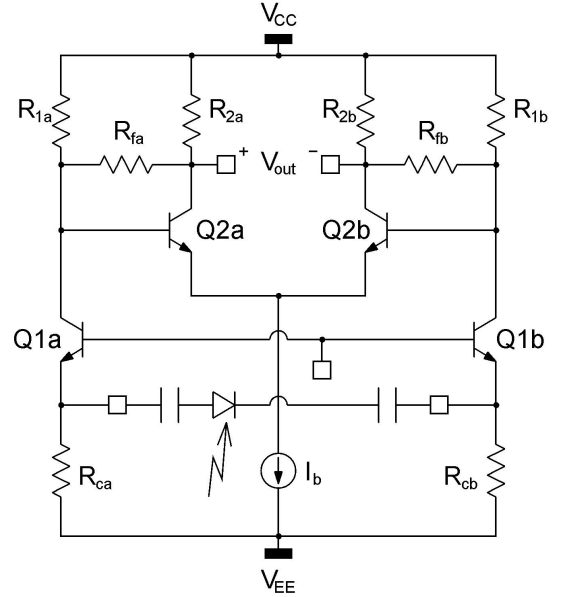


Fig. 7: Differential bipolar transimpedance amplifier.

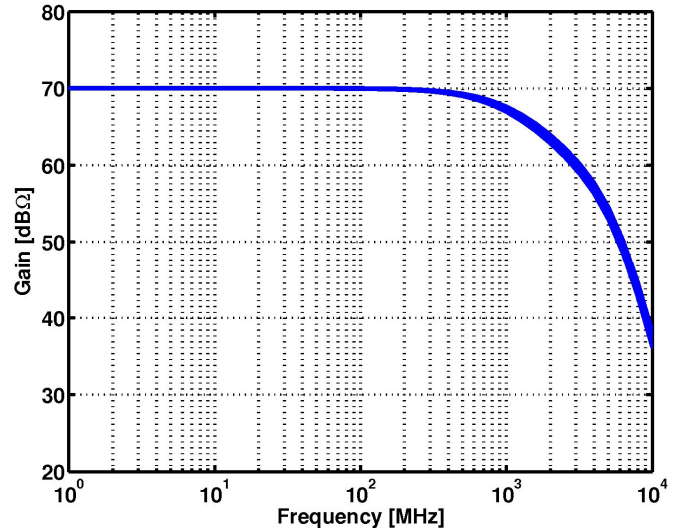


Fig. 8: Bode diagram of the closed loop transimpedance gain of the circuit for total ionizing dose going from 0 to 300 kGy.

Fig. 8 shows the simulated transimpedance gain of the circuit as a function of frequency for TID values going from 0 to 300 kGy. The DC gain is seen to stay constant at 70 dB Ω , or roughly 3.2 k Ω . As the ionizing dose increases the bandwidth of the circuit reduces with about 6 % from 1.05 GHz to 990 MHz. After 200 kGy it increases again. The main origin of this behavior lies in the reduction in current through Q_2 by an increased base current drawn from the current mirrors as described earlier for the VCSEL driver.

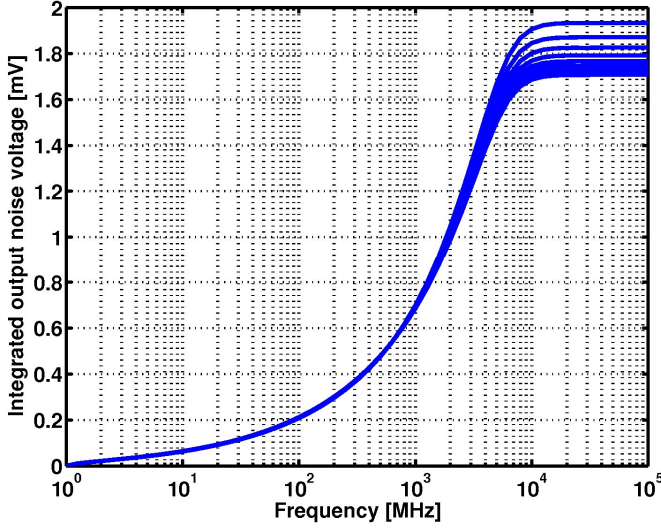


Fig. 9: Rms integrated output noise voltage of the transimpedance amplifier for TID values from 0 Gy to 300 kGy.

The rms integrated output noise voltage for increasing frequency is depicted in Fig. 9. The upper curve shows the curve before irradiation. As the total dose increases the integrated noise reduces mostly owing to the reduction in bandwidth described previously. The sensitivity of the circuit can be evaluated by dividing the total integrated output noise voltage by the transimpedance gain of the circuit. An input current sensitivity of about 2 μ A is achieved for a SNR of 10 dB.

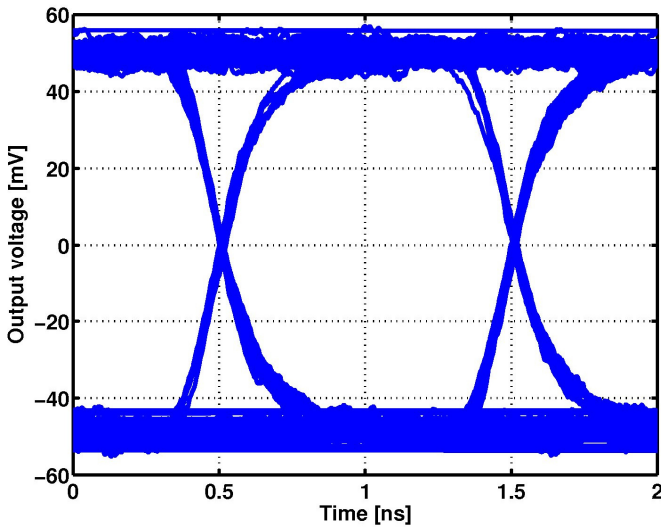


Fig. 10: Eye-diagram of the output voltage from a noise-transient simulation of the transimpedance amplifier for a 1 Gbps 2^7 -1 PRBS input current of 30 μ A.

A combined noise transient simulation was used to verify the behavior of the driver at different dose levels and for different currents. No significant degradation is observed in these simulations. An eye diagram of the output signal is shown in Fig. 10, where the input was a 1 Gbps 2^7 -1 PRBS current of 30 μ A.

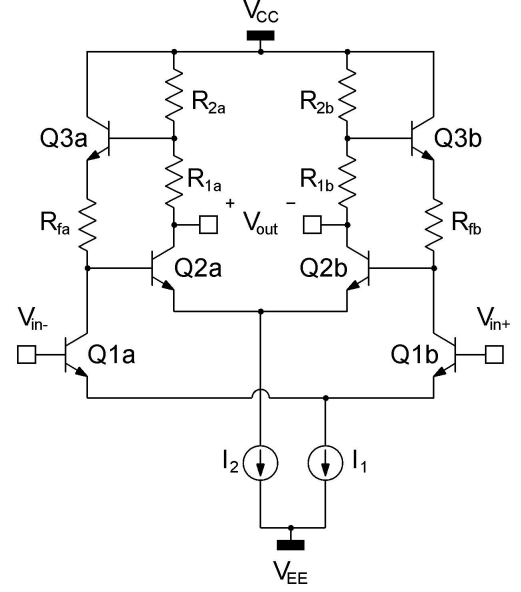


Fig. 11: Differential bipolar Cherry-Hooper amplifier stage.

Fig. 11 depicts the simplified schematic of a differential bipolar Cherry-Hooper stage proposed as building block for the post-amplifier in the receiver. The circuit shows many similarities with the transimpedance amplifier discussed previously. The construction of a Cherry-Hooper amplifier is based on a transconductance stage followed by a transimpedance stage. The reduced input impedance of the transimpedance amplifier ensures a high circuit bandwidth albeit with a moderate amplifier gain. In the presented circuit the transconductance stage is formed by Q_1 in common-emitter configuration and is followed by Q_2 , also in common-emitter configuration and with negative shunt-shunt feedback provided by emitter-follower Q_3 and R_f . The sensed feedback voltage is divided from the output voltage in order to reduce the loop gain. This in turn increases the overall closed loop gain of the entire circuit:

$$A_v = g_{m1} R_f \left(1 + \frac{R_1}{R_2} \right). \quad (3)$$

The bandwidth of the circuit is mostly determined by the pole at the base node of Q_2 and can be approximated by

$$BW = \frac{1 + g_{m2} R_2}{2\pi C_{b2} R_f}. \quad (4)$$

This equation reveals the drawback of adding the resistive divider as R_2 must be chosen smaller since part of the DC voltage drop is now taken by R_1 . Basically this technique allows to trade gain for bandwidth and vice versa.

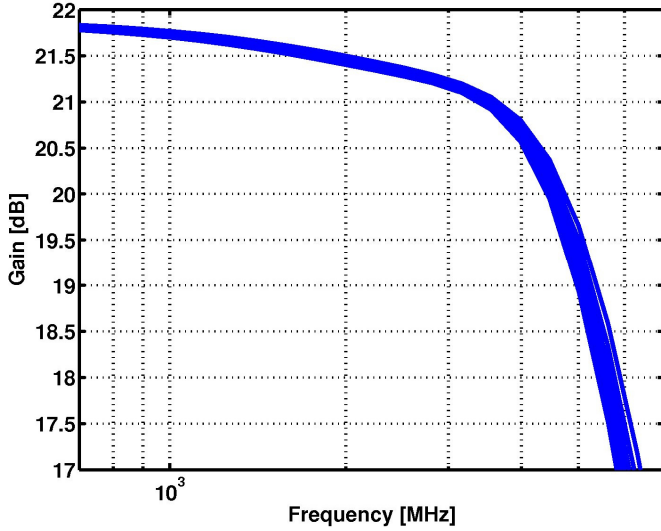


Fig. 12: Bode diagram of the closed loop voltage gain of the Cherry-Hooper circuit for total ionizing dose going from 0 to 300 kGy.

Fig. 12 shows the voltage gain of the amplifier stage as a function of frequency for total ionizing dose levels from 0 Gy up to 300 kGy. With respect to the bandwidth of the circuit, the same behavior is observed as described for the transimpedance amplifier, i.e. an initial reduction followed by recovery owing to a reduced current through the amplifying device. In this circuit however also a minor gain degradation is observed owing to the dependence of the gain on g_{m1} and hence on the current through Q_1 which is degraded in the same manner as Q_2 . The gain remains between 21.5 dB and 22 dB and the bandwidth stays larger than 5 GHz inspite of radiation.

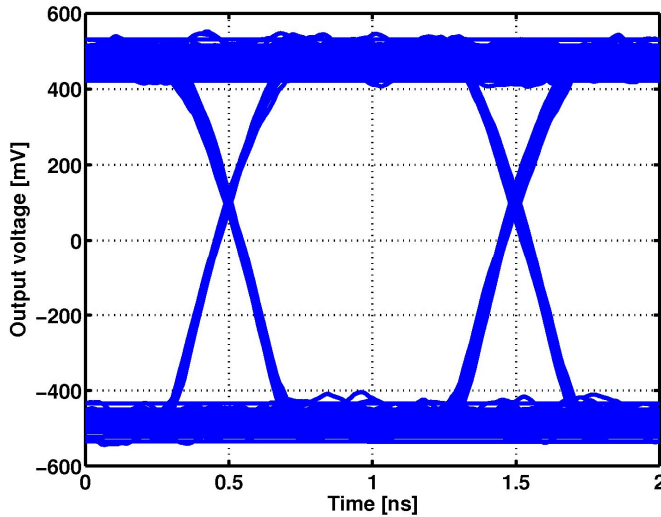


Fig. 13: Eye-diagram of the output voltage from a noise-transient simulation of the Cherry-Hooper amplifier for a 1 Gbps 2^7 -1 PRBS input current of 30 μ A.

A noise transient analysis was performed on the cascade of the transimpedance and Cherry-Hooper amplifier and a typical result is shown in Fig. 13. The same input current of 30 μ A was used as for the TIA alone. Notice by comparison with Fig. 10 that the SNR of the signal is almost not degraded by the post-amplifier owing to the large gain of the TIA. Results with increasing dose levels are similar.

IV. CONCLUSION

We have presented recent design and characterization results on the most critical electronic building blocks in a MGy radiation tolerant optoelectronic transceiver for application in ITER. All circuits were designed in a 0.35 μ m SiGe BiCMOS technology using only the npn HBT devices. Simulations were performed using the model provided by the manufacturer but adapted to include their radiation dependent current gain degradation.

At the transmitter side, a VCSEL driver has been designed, simulated and measured before, during and after irradiation up to 1.6 MGy. No significant degradation is seen up to these dose levels and for a bitrate up to 622 Mbps.

At the receiver side a fully differential transimpedance amplifier has been designed and simulated. The circuit features a gain of 3.2 k Ω , a bandwidth of 1 GHz and an input current sensitivity of 2 μ A at an SNR of 10 dB. The TIA is followed by a Cherry-Hooper based differential amplifier with a voltage gain of more than 21 dB and a bandwidth surpassing 5 GHz. Both circuits feature a degradation of only a few percent for a gamma dose up to 600 kGy.

V. REFERENCES

- [1] "EFDA Task TW1-TVA/RADTOL - Radiation Tolerance Assessment of Remote Handling Components - Final Progress Report European Home Team", compiled by M. Van Uffelen, Report R-3715, Dec. 2002.
- [2] J. Palmer, P. Agostini, R. Gottfried, M. Irving, E. Martin, M. Siuko, A. Tesini, M. Van Uffelen, "Remote Maintenance of the ITER Divertor", presented at the "10th International Conference on Robotics and Remote Systems", Gainesville (Florida, USA), March 2004.
- [3] J.-G. Zhang, A.B. Sharma, M. Kaewnin, "Proposed optical fibre system using pulse width and amplitude modulation for hybrid analogue/digital transmission", *Opt. Eng.*, Vol. 37, N°1, pp 215-219, 1998.
- [4] M. Van Uffelen, A. Fernandez Fernandez, B. Brichard, F. Berghmans, M. Decréton, "Radiation tolerance qualification for maintenance tasks in the future fusion reactors: from fibre-optic components to robust data links", *Fusion Engineering and Design*, n°69, pp. 191-195, 2003.
- [5] P. Leroux, M. Van Uffelen, F. Berghmans, E. Simoen, C. Claeys, "A Compact, Broad-range, Physical SPICE Model Extension for the γ -radiation Induced β -degradation in a Discrete SiGe HBT", in *Proceedings RADECS*, September, 2006.
- [6] P. Leroux, M. Van Uffelen, F. Berghmans, A. Giraud, "Design and Assessment of a High Gamma-Dose Tolerant VCSEL Driver with Discrete SiGe HBT's", *IEEE Trans. Nucl. Sci.*, Vol. 53, No. 4, pp. 2033-2039, 2006.
- [7] X. Montagner, R. Briand, P. Fouillat, R.D. Schrimpf, A. Touboul, K.F. Galloway, M.C. Calvet, P. Calve, "Dose-rate and irradiation temperature dependence of BJT SPICE modelrad-parameters", in *Proceedings RADECS*, September, 1997.
- [8] Y. Deng et al., "SPICE Modeling of Neutron Displacement Damage and Annealing Effects in Bipolar Junction Transistors", *IEEE Trans. Nucl. Sci.*, Vol. 50, pp. 1873-1877, Dec. 2003.
- [9] J.D. Cressler, G. Niu, "Silicon-Germanium Heterojunction Bipolar Transistors", Artech House, Norwood MA, 2003.
- [10] J. Babcock et al., "Ionizing Radiation Tolerance of High-Performance SiGe HBT's Grown by UHV/CVD", *IEEE Trans. Nucl. Sci.*, Vol. 42, N°6, pp. 1558-1566, 1995.
- [11] S. Put, E. Simoen, S. Van Huylenbroeck, C. Claeys, M. Van Uffelen and P. Leroux, "Effect of airgap deep trench isolation on the gamma radiation behavior of a 0.13 μ m SiGe:C NPN HBT technology", in *Proceedings RADECS*, September, 2008.
- [12] P. Leroux, W. De Cock, M. Van Uffelen and M. Steyaert, "Design, Assessment and Modeling of an Integrated 0.4 μ m SiGe Bipolar VCSEL Driver under γ -Radiation", in *Proc. RADECS*, September, 2008.